

Active manifold learning via a unified framework for manifold landmarking

Hongteng Xu, Licheng Yu, Mark A. Davenport, *Senior Member, IEEE*, Hongyuan Zha

Abstract—The success of semi-supervised manifold learning is highly dependent on the quality of the labeled samples. Active manifold learning aims to select and label representative landmarks on a manifold from a given set of samples to improve semi-supervised manifold learning. In this paper, we propose a novel active manifold learning method based on a unified framework of manifold landmarking. In particular, our method combines geometric manifold landmarking methods with algebraic ones. We achieve this by using the Gershgorin circle theorem to construct an upper bound on the learning error that depends on the landmarks and the manifold's alignment matrix in a way that captures both the geometric and algebraic criteria. We then attempt to select landmarks so as to minimize this bound by iteratively deleting the Gershgorin circles corresponding to the selected landmarks. We also analyze the complexity, scalability, and robustness of our method through simulations, and demonstrate its superiority compared to existing methods. Experiments in regression and classification further verify that our method performs better than its competitors.

Index Terms—Semi-supervised manifold learning, active learning, manifold landmarking, Gershgorin circle theorem.

I. INTRODUCTION

SEMI-SUPERVISED manifold learning methods [1]–[5] have been widely used to capture low-dimensional structure in high-dimensional data. These methods take semantic information (labels) into consideration when learning the mapping from the ambient space to the latent space. The learned latent variables can be used as features for many learning tasks [1], [4], [6]. In some cases [2], [3], we are even able to learn the mapping from the ambient space to the label space directly and estimate the labels for the complete data set.

An interesting and important problem in the context of semi-supervised manifold learning is *how to select landmarks from a large number of unlabeled samples to minimize the learning error for the remaining samples*. This problem is very common in practical situations — given a large number of unlabeled samples, we can often label only a few of them because of limitations in budget, time, and other resources. Some typical examples where this arises include:

- **Image classification.** Given a large number of unlabeled images, we generally have very limited human resources with which to label them. A more practical strategy

is labeling a subset of the images and applying semi-supervised learning methods to classify the remaining unlabeled ones. The challenge is to select which images to label in order to achieve the best classifier.

- **Network management and information diffusion.** In a social network, advertisers with limited budgets need to select influential users in order to disseminate advertising and promotional information efficiently. The challenge is how to identify and select users to improve and accelerate the spread of information.
- **Smart buildings.** In a smart building we need to distribute sensors, e.g., surveillance cameras or environmental sensors, with a limited budget. If each sensor can only detect anomalies in a small region, the challenge is how to assign their locations to maximize their coverage.

We can view these and similar problems as “active manifold learning” problems [7], [8], where the goal is to select representative landmarks for semi-supervised manifold learning.

In this paper, we propose a novel landmarking algorithm combining geometric landmarking methods with algebraic ones. Specifically, we first give a bound on the learning error of semi-supervised manifold learning based on the manifold's alignment matrix. Then, we show that many existing methods actually minimize the bound via different but one-sided strategies, which can be unified into a common algorithmic framework. We propose a computationally-friendly surrogate for the error bound based on the Gershgorin circle theorem [9], which is used as the objective function for active manifold learning. We then propose a heuristic but effective landmark selection algorithm, which selects landmarks via deleting and updating the Gershgorin circles iteratively, where the indices of deleted circles corresponds to landmarks. We analyze the complexity, scalability, and robustness of our algorithm and demonstrate its superiority to the existing state-of-art landmarking methods.

The contributions of our work are three-fold. First, we explore properties of manifold learning and semi-supervised manifold learning and propose a unified framework of manifold landmarking for active manifold learning. Second, in the proposed framework, we analyze existing manifold landmarking methods in depth and propose an active manifold learning algorithm that can be viewed as a generalization and unification of existing methods. Third, we propose a Gershgorin circle-based landmarking algorithm with low computational complexity and high scalability that achieves encouraging results in both regression and classification tasks.

The remainder of this paper is organized as follows. We first introduce related work and background on manifold learning, semi-supervised manifold learning, and active learning in

H. and M. A. Davenport are with the Department of Electrical and Computer Engineering, Georgia Institute of Technology, Atlanta, GA, 30332 USA (e-mail: {hxd42, mdav}@gatech.edu).

L. Yu is with the Department of Computer Science, University of North Carolina at Chapel Hill, Chapel Hill, NC, 27599 USA (e-mail: licheng@cs.unc.edu).

H. Zha is with the College of Computing, Georgia Institute of Technology, Atlanta, GA, 30332 USA (e-mail: zha@cc.gatech.edu).

Section II. Section III provides an analysis of existing manifold landmarking methods and constructs our unified framework. Section IV contains a derivation of our proposed method for active manifold learning based on this unified framework and a comparison of this method to existing approaches. Experiments and discussion are provided in Section V. Finally, Section VI concludes the paper. The Appendix contains additional technical details.

II. RELATED WORK AND BACKGROUND

A. Manifold learning

Manifold models arise in a wide variety of signal processing and machine learning problems, and manifold learning serves as an important tool in applications such as computer vision and imaging [10]–[13], array signal processing [14]–[16], and graph-based signal analysis [17]–[19], just to name a few. Many manifold learning methods are based on the assumption of local linearity. For example, assuming that each data point can be linearly represented by its neighbors, the locally linear embedding (LLE) [20] finds the linear coefficients that reconstruct each data point from its neighbors and aligns them globally. Similarly, local tangent space alignment (LTSA) [21] constructs an approximation of the local tangent space at each data point and aligns these tangent spaces in a global latent space. Other methods aim to preserve the distance between samples in the latent space. The ISOMAP [22] method aims to preserve the geodesic distance between points in the latent space. The Laplacian Eigenmap (LE) [23], [24] and the diffusion map [25], [26] describe a manifold by a Laplacian graph matrix, which ensures the pairwise distances between samples and their neighbors are inherited by the latent variables.

All of these algorithms can be unified into the framework of a common eigenvalue problem [2], [8], [27]. Specifically, let $\mathbf{X} = [\mathbf{x}_1, \dots, \mathbf{x}_N] \in \mathbb{R}^{D \times N}$ be samples of a manifold \mathcal{X} . The manifold learning methods above find a low-dimensional representation of \mathbf{X} , denoted as $\mathbf{Y} = [\mathbf{y}_1, \dots, \mathbf{y}_N] \in \mathbb{R}^{d \times N}$ ($d \ll D$), by solving

$$\begin{aligned} \min_{\mathbf{Y}} \text{tr}(\mathbf{Y}\Phi\mathbf{Y}^T) \\ \text{s.t. } \mathbf{Y}\mathbf{Y}^T = \mathbf{I}_d. \end{aligned} \quad (1)$$

Here $(\cdot)^T$ is the transpose of matrix, $\text{tr}(\cdot)$ calculates the trace of matrix, and \mathbf{I}_d is a $d \times d$ identity matrix. The matrix $\Phi \in \mathbb{R}^{N \times N}$ is defined on a K -nearest neighbors (K -NN) graph derived from \mathbf{X} . Φ can be the Laplacian graph in LE, a variant of the Laplacian graph in diffusion maps, or the alignment matrix in ISOMAP, LLE, or LTSA. In this paper, we call Φ the alignment matrix. The derivations of Φ for various manifold learning methods are given in Appendix A.

B. Semi-supervised manifold learning

The methods mentioned above are unsupervised. When a subset of samples are labeled, we can extend these methods to semi-supervised manifold learning and estimate labels for the remaining unlabeled samples. In particular, let $\mathbf{X} = [\mathbf{X}_{\mathcal{L}}, \mathbf{X}_{\bar{\mathcal{L}}}]$, where \mathcal{L} is the index set of the labeled samples with cardinality $|\mathcal{L}| = L$ and $\bar{\mathcal{L}} = \{1, \dots, N\} \setminus \mathcal{L}$ is the index set of

the unlabeled samples. Given $\mathbf{X}_{\mathcal{L}}$ and labels $\mathbf{Z}_{\mathcal{L}}$, the goal of semi-supervised manifold learning is to determine the labels $\mathbf{Z}_{\bar{\mathcal{L}}}$ of the unlabeled samples $\mathbf{X}_{\bar{\mathcal{L}}}$ by exploiting the underlying manifold structure [1]–[3], [5].

Semi-supervised manifold learning methods can be broadly divided into two classes. The simplest methods are extremely straightforward and proceed by attempting to learn the mapping from the ambient space \mathcal{X} to the label space \mathcal{Z} directly. A typical example is the Least Squares (LS) method in [2], which considers a problem of the form

$$\min_{\mathbf{Z}_{\bar{\mathcal{L}}}} \text{tr} \left([\mathbf{Z}_{\mathcal{L}}, \mathbf{Z}_{\bar{\mathcal{L}}}] \begin{bmatrix} \Phi_{\mathcal{L}\mathcal{L}} & \Phi_{\mathcal{L}\bar{\mathcal{L}}} \\ \Phi_{\bar{\mathcal{L}}\mathcal{L}} & \Phi_{\bar{\mathcal{L}}\bar{\mathcal{L}}} \end{bmatrix} \begin{bmatrix} \mathbf{Z}_{\mathcal{L}}^T \\ \mathbf{Z}_{\bar{\mathcal{L}}}^T \end{bmatrix} \right) + \underbrace{\gamma \|\mathbf{Z}_{\bar{\mathcal{L}}}\|_F^2}_{\text{optional}}, \quad (2)$$

where the first term of (2) enforces a manifold structure on \mathbf{Z} (estimated from \mathbf{X}) and the second term of (2) is an optional regularizer on the Frobenius norm of $\mathbf{Z}_{\bar{\mathcal{L}}}$.

The second class of methods consists of decomposing the mapping $\mathcal{X} \mapsto \mathcal{Z}$ into two mappings: a mapping from the ambient space \mathcal{X} to the latent space \mathcal{Y} and a mapping from the latent space \mathcal{Y} to the label space \mathcal{Z} . For example, the spectral method (Spec) in [3] assumes that both the data manifold and the label manifold are different images of the same latent space: $\mathcal{X} = h(\mathcal{Y})$ and $\mathcal{Z} = g(\mathcal{Y})$. The mapping $g : \mathcal{Y} \rightarrow \mathcal{Z}$ is assumed to be an affine transformation and the $\mathbf{Y} \subset \mathcal{Y}$ is learned by traditional manifold learning algorithm with a label-based regularizer:

$$\begin{aligned} \min_{\mathbf{Y}} \text{tr}(\mathbf{Y}\Phi\mathbf{Y}^T) + \gamma \text{tr}(\mathbf{Y}_{\mathcal{L}}\mathbf{G}\mathbf{Y}_{\mathcal{L}}^T) \\ \text{s.t. } \mathbf{Y}\mathbf{Y}^T = \mathbf{I}_d, \end{aligned} \quad (3)$$

where \mathbf{G} is the orthogonal projection whose null space is spanned by $[\mathbf{1}, \mathbf{Z}_{\mathcal{L}}^T]$. After obtaining \mathbf{Y} , we then learn an affine transformation between $\mathbf{Y}_{\mathcal{L}}$ and $\mathbf{Z}_{\mathcal{L}}$.

This more general approach to semi-supervised manifold learning essentially treats the learned latent variables as features which can be used as inputs to a traditional learning algorithm. This paradigm can be extended to a variety of more complex dimensionality reduction techniques and learning algorithms that incorporate manifold regularizers [1], [4], [6]. Take the manifold-regularized sparse coding model [4], [6] as one example. Here, given a set of samples \mathbf{X} , a dictionary \mathbf{D} and sparse codes \mathbf{Y} are learned by

$$\min_{\mathbf{D}, \mathbf{Y}} \underbrace{\|\mathbf{X} - \mathbf{D}\mathbf{Y}\|_F^2}_{\text{sparse coding}} + \gamma_1 \|\mathbf{Y}\|_1 + \underbrace{\gamma_2 \text{tr}(\mathbf{Y}\Phi\mathbf{Y}^T)}_{\text{manifold regularizer}}, \quad (4)$$

where the third term is an alignment matrix-based regularizer. Sparse coding with a manifold regularizer combine to produce features \mathbf{Y} that simultaneously provide a sparse representation and also respect the manifold structure in the data. After learning $\mathbf{Y}_{\mathcal{L}}$, a classifier can be trained on the labeled data $\{\mathbf{Y}_{\mathcal{L}}, \mathbf{Z}_{\mathcal{L}}\}$.

C. Active learning

Active learning [28]–[30] has been used to select representative samples [31]–[33] and improve learning results in many applications ranging from computer vision [34],

Algorithm 1 Active Manifold Learning**Input:** $\mathbf{X} = [\mathbf{x}_i] \in \mathbb{R}^{D \times N}$, the number of landmarks L .**Output:** Labels $\mathbf{Z} = [\mathbf{Z}_{\mathcal{L}}, \mathbf{Z}_{\bar{\mathcal{L}}}] \in \mathbb{R}^{d \times N}$.

- 1: Generate Φ via any manifold learning algorithm.
- 2: Apply a landmark selection algorithm to choose \mathcal{L} .
- 3: Label $\{\mathbf{x}_i\}_{i \in \mathcal{L}}$ with $\mathbf{Z}_{\mathcal{L}}$.
- 4: *For learning labels:*
- 5: Apply SSML to $\{\mathbf{X}, \mathbf{Z}_{\mathcal{L}}\}$.
- 6: *For manifold-regularized tasks:*
- 7: Learn features \mathbf{Y} and train model with $\{\mathbf{Y}_{\mathcal{L}}, \mathbf{Z}_{\mathcal{L}}\}$.
- 8: Return estimated labels $\mathbf{Z}_{\bar{\mathcal{L}}}$ for $\{\mathbf{x}\}_{i \in \bar{\mathcal{L}}}$.

natural language processing [35], speech recognition [36], data mining [37], and geoscience [38], [39], and many more.

From the viewpoint of active learning [7], [40], the challenge of active manifold learning is to select which samples on the manifold to label in order to minimize the learning error on the remaining samples. Following [2], [8], our approach to active manifold learning is to combine a landmark selection algorithm with semi-supervised manifold learning or manifold regularization. This is summarized in Algorithm 1.

This problem is very close to manifold landmarking, where the aim is to select representative samples on a manifold, but where the selection criterion is driven more by the goal of preserving structural or geometric information about the target manifold (see, for example, the methods in [41]–[43]). The concerns that arise in the semi-supervised setting are not necessarily limited to simply preserving the geometric structure – nevertheless, we will see that manifold landmarking methods can play an important role in the active manifold learning problem. Below we will describe two broad categories of landmarking methods which we denote *algebraic* and *geometric* methods, and then show that they can be unified into a common framework for active manifold learning.

III. A UNIFIED FRAMEWORK FOR MANIFOLD LANDMARKING

A. Algebraic methods

In [8] we recently proposed a manifold landmarking method (called **MinCond**) based on an algebraic analysis of semi-supervised manifold learning that aims to approximately minimize the condition number of the alignment matrix. This method is motivated by the approaches to semi-supervised manifold learning in (2) and (3). In particular, if we denote the objective function in (2) as $f(\mathbf{Z})$ and set the gradient of $f(\mathbf{Z})$ with respect to the labels $\mathbf{Z}_{\bar{\mathcal{L}}}$ to be zero, i.e., $\frac{\partial f(\mathbf{Z})}{\partial \mathbf{Z}_{\bar{\mathcal{L}}}} = \mathbf{0}$, we can obtain a closed-form solution for $\mathbf{Z}_{\bar{\mathcal{L}}}$ by solving the following linear system of equations:

$$(\Phi_{\bar{\mathcal{L}}\bar{\mathcal{L}}} + \gamma \mathbf{I}_{N-L}) \mathbf{Z}_{\bar{\mathcal{L}}}^T = \Phi_{\bar{\mathcal{L}}\mathcal{L}} \mathbf{Z}_{\mathcal{L}}^T. \quad (5)$$

One can also consider the Lagrangian function of (3) with a Lagrange multiplier β , i.e., $\text{tr}(\mathbf{Y}\Phi\mathbf{Y}^T) + \gamma \text{tr}(\mathbf{Y}_{\mathcal{L}}\mathbf{G}\mathbf{Y}_{\mathcal{L}}^T) + \beta \mathbf{1}_d^T \mathbf{Y} \mathbf{Y}^T \mathbf{1}_d - \beta d$, where $\mathbf{1}_d$ is a d -dimensional vector of ones, and set the gradient of the Lagrangian function with respect to the unknown latent variables $\mathbf{Y}_{\bar{\mathcal{L}}}$ to be zero, yielding

$$(\Phi_{\bar{\mathcal{L}}\bar{\mathcal{L}}}) \mathbf{Y}_{\bar{\mathcal{L}}}^T + 2\beta \mathbf{Y}_{\bar{\mathcal{L}}}^T (\mathbf{1}_d \mathbf{1}_d^T) = \Phi_{\bar{\mathcal{L}}\mathcal{L}} \mathbf{Y}_{\mathcal{L}}^T. \quad (6)$$

Note that if we ignore the effect of the optional regularizer and the Lagrange multiplier (i.e., set γ, β , which can typically be set quite small, to zero), then (6) is equivalent to (5). Thus, although the analysis below is for (2), it can also apply to (3) by simply replacing $\mathbf{Z}_{\bar{\mathcal{L}}}$ with $\mathbf{Y}_{\bar{\mathcal{L}}}$ throughout.

In practice, we typically expect the observations \mathbf{X} to be somewhat noisy. In this case, we can treat the corresponding alignment matrix Φ as being also contaminated with noise, in which case (5) becomes

$$(\Phi_{\bar{\mathcal{L}}\bar{\mathcal{L}}} + \mathbf{E}_2) \hat{\mathbf{Z}}_{\bar{\mathcal{L}}}^T = (\Phi_{\bar{\mathcal{L}}\mathcal{L}} + \mathbf{E}_1) \mathbf{Z}_{\mathcal{L}}^T, \quad (7)$$

where $\mathbf{E}_1, \mathbf{E}_2$ are noise matrices and $\hat{\mathbf{Z}}_{\bar{\mathcal{L}}}$ is our estimate of the $\mathbf{Z}_{\bar{\mathcal{L}}}$ that one would obtain using the “noise-free” Φ .

As shown in [8], [44], the relative error between our estimate $\hat{\mathbf{Z}}_{\bar{\mathcal{L}}}$ and the “noise-free” estimate $\mathbf{Z}_{\bar{\mathcal{L}}}$ is bounded by

$$\begin{aligned} \frac{\|\mathbf{Z}_{\bar{\mathcal{L}}} - \hat{\mathbf{Z}}_{\bar{\mathcal{L}}}\|_2}{\|\mathbf{Z}_{\bar{\mathcal{L}}}\|_2} &\leq \kappa(\Phi_{\bar{\mathcal{L}}\bar{\mathcal{L}}}) \left(\frac{\|\mathbf{E}_1\|_2}{\|\Phi_{\bar{\mathcal{L}}\mathcal{L}}\|_2} + \frac{\|\mathbf{E}_2\|_2}{\|\Phi_{\bar{\mathcal{L}}\bar{\mathcal{L}}}\|_2} \right) \\ &\leq \epsilon \kappa(\Phi_{\bar{\mathcal{L}}\bar{\mathcal{L}}}) \left(\frac{1}{\|\Phi_{\bar{\mathcal{L}}\mathcal{L}}\|_2} + \frac{1}{\|\Phi_{\bar{\mathcal{L}}\bar{\mathcal{L}}}\|_2} \right), \end{aligned} \quad (8)$$

where $\|\cdot\|_2$ is the induced ℓ_2 matrix norm, $\kappa(\cdot)$ computes the condition number, and $\epsilon = \max(\|\mathbf{E}_1\|_2, \|\mathbf{E}_2\|_2)$. Because the relative learning error is directly related to $\kappa(\Phi_{\bar{\mathcal{L}}\bar{\mathcal{L}}})$, MinCond aims to select landmarks by deleting L rows/columns of Φ so that the remaining principal submatrix $\Phi_{\bar{\mathcal{L}}\bar{\mathcal{L}}}$ has the smallest possible condition number:

$$\begin{aligned} \min_{\mathcal{L}} \kappa(\Phi_{\bar{\mathcal{L}}\bar{\mathcal{L}}}) \\ \text{s.t. } |\mathcal{L}| = L. \end{aligned} \quad (9)$$

Traditional condition number minimization algorithms such as [45]–[48] require the feasible domain to be a compact convex set of the cone of positive semidefinite matrices, which is not available for (9). Generally, (9) can be solved approximately by the Rank-revealing QR-factorization (RRQR) in [49]. In Appendix B, we demonstrate that RRQR can give an upper bound on the solution of (9). However, the bound is too loose for practical application. In practice, MinCond reformulates the problem from minimizing the condition number of the alignment matrix to minimizing the dynamic range of the eigenvalues of the logarithmic alignment matrix and deletes the rows/columns of the alignment matrix iteratively. Specifically, the logarithmic version of the objective function in (9) is

$$|\ln \lambda_{\max}(\Phi_{\bar{\mathcal{L}}\bar{\mathcal{L}}}) - \ln \lambda_{\min}(\Phi_{\bar{\mathcal{L}}\bar{\mathcal{L}}})|. \quad (10)$$

Here, $\ln \lambda_{\max}$ and $\ln \lambda_{\min}$ are the largest and the smallest eigenvalues of $\ln(\Phi_{\bar{\mathcal{L}}\bar{\mathcal{L}}})$. Instead of minimizing the dynamic range of the eigenvalues directly, we minimize an upper bound. Specifically, the objective function becomes

$$|\Lambda_u(\Phi_{\bar{\mathcal{L}}\bar{\mathcal{L}}}) - \Lambda_l(\Phi_{\bar{\mathcal{L}}\bar{\mathcal{L}}})|, \quad (11)$$

where $\Lambda_u(\Phi_{\bar{\mathcal{L}}\bar{\mathcal{L}}})$ and $\Lambda_l(\Phi_{\bar{\mathcal{L}}\bar{\mathcal{L}}})$ are upper and lower bounds on the eigenvalues of $\ln(\Phi_{\bar{\mathcal{L}}\bar{\mathcal{L}}})$, which are computed according to the Gershgorin circles of $\ln(\Phi_{\bar{\mathcal{L}}\bar{\mathcal{L}}})$. By deleting the Gershgorin circles of $\ln(\Phi_{\bar{\mathcal{L}}\bar{\mathcal{L}}})$ iteratively, we can shrink the interval $[\Lambda_u, \Lambda_l]$, which bounds the condition number accordingly. The samples corresponding to deleted circles are the selected landmarks. Further details of MinCond can be found in [8].

B. Geometric methods

Many other manifold landmarking methods have a more geometric flavor. Representative methods include a geodesic distance-based algorithm (**MaxMinGeo**) [41], [42] and a determinantal point process-based algorithm (**DPP**) [43]. MaxMinGeo and DPP aim to distribute the landmarks to maximize the coverage of the landmarks on the target manifold by ensuring that the landmarks are not too close in the ambient space. Denote the distance (under a given metric) between samples \mathbf{x}_i and \mathbf{x}_j as d_{ij} . Mathematically, the problem of maximizing the minimum distance between landmarks can be written as

$$\begin{aligned} \max_{\mathcal{L}} \min_{i,j \in \mathcal{L}} d_{ij} \\ \text{s.t. } |\mathcal{L}| = L, \end{aligned} \quad (12)$$

where \mathcal{L} is the set of landmarks. MaxMinGeo tries to solve this problem approximately in a heuristic way. In particular, MaxMinGeo first initializes several landmarks (or one landmark) randomly, and then it adds new landmarks iteratively and ensures that the minimum geodesic distance between the new landmark and existing ones is maximized.

To further accelerate manifold landmarking, the DPP method makes an additional concession. Instead of maximizing the minimum distance between two arbitrary landmarks, the DPP method simply ensures that the selection of the new landmark is performed using a probabilistic distribution that suppresses the probability of selecting existing landmarks' neighbors. As a result, the landmarks will tend to not be neighbors of each other. In Section V, we will show that the DPP method achieves comparable performance to MaxMinGeo using much less runtime, which can be viewed as an approximate but fast implementation of MaxMinGeo.

Both of these methods can be viewed as heuristics for attempting to approximately maximize the coverage of the landmarks on the target manifold by ensuring that once a landmark is selected, we use the opportunity to select additional landmarks to gain a higher degree of coverage of the manifold by avoiding the immediate neighbors of the landmarks selected up to that point. When the distance between samples is defined on a K -NN graph of samples, the strategy of these methods can be re-interpreted based on the alignment matrix. Specifically, the alignment matrices in LE, LLE, and LTSA have the following Property, which we prove in Appendix C:

Property 1. For the $\Phi = [\phi_{ij}]$ in LE, LLE, and LTSA, $\phi_{ij} \neq 0$ if and only if samples \mathbf{x}_i and \mathbf{x}_j are neighbors in the K -NN graph.

For example, LE uses a Laplacian graph matrix as the alignment matrix. The entry $\phi_{ij} = -d_{ij}$ if samples \mathbf{x}_i and \mathbf{x}_j are neighbors, otherwise $\phi_{ij} = 0$. $\phi_{ii} = \sum_j d_{ij}$.

In this setting, the implicit goal of geometric methods that the landmarks should maximize the coverage of the landmarks on the target manifold can be achieved when the submatrix $\Phi_{\bar{\mathcal{L}}\mathcal{L}}$ has as many nonzeros as possible. In other words, we would like to ensure that each landmark in \mathcal{L} has many direct

connections in the K -NN graph to elements in $\bar{\mathcal{L}}$. One way to achieve this goal is to solve the optimization problem

$$\begin{aligned} \max_{\mathcal{L}} \max_{j \in \bar{\mathcal{L}}} \|\phi_j\|_0 \\ \text{s.t. } |\mathcal{L}| = L, \end{aligned} \quad (13)$$

where ϕ_j is the column of $\Phi_{\bar{\mathcal{L}}\mathcal{L}}$ corresponding to the index j and $\|\cdot\|_0$ is the so-called " ℓ_0 norm", which counts the number of nonzero elements in a vector. This objective function encourages the selection of landmarks which are densely connected to elements in $\bar{\mathcal{L}}$.

Solving (13) directly is intractable. Therefore, in this work we further relax the objective function from the ℓ_0 -norm to the ℓ_1 matrix norm, i.e., $\|\Phi_{\bar{\mathcal{L}}\mathcal{L}}\|_1 = \max_{j \in \bar{\mathcal{L}}} \sum_{i \in \mathcal{L}} |\phi_{ij}|$. Finally, note that

$$\max_{\mathcal{L}} \|\Phi_{\bar{\mathcal{L}}\mathcal{L}}\|_1 \Leftrightarrow \min_{\mathcal{L}} \frac{1}{\|\Phi_{\bar{\mathcal{L}}\mathcal{L}}\|_1}. \quad (14)$$

C. A unified algorithmic framework

As seen above, different viewpoints on landmarking methods actually lead to very different criteria for landmark selection. On the one hand, the algebraic method focuses on minimizing learning error for the remaining samples by minimizing the condition number of the remaining principal submatrix (i.e., MinCond). On the other hand, the geometric methods focus on maximizing the diversity of the landmarks. Under certain metrics, the minimum distance between landmarks is maximized deterministically (i.e., MaxMinGeo) or probabilistically (i.e., DPP) to ensure that the landmarks have a good coverage on the target manifold. Based on the analysis in Section III-A and III-B, we can unify these two kinds of methods into a single algorithmic framework.

Towards this end, we first note that we can further bound the right-hand side of (8) via the standard norm inequality for an $M \times N$ matrix \mathbf{A} of $\|\mathbf{A}\|_1 \leq \sqrt{M}\|\mathbf{A}\|_2$, yielding

$$\frac{\|\mathbf{Z}_{\bar{\mathcal{L}}\mathcal{L}} - \hat{\mathbf{Z}}_{\bar{\mathcal{L}}\mathcal{L}}\|_2}{\|\mathbf{Z}_{\bar{\mathcal{L}}\mathcal{L}}\|_2} \leq \epsilon \kappa(\Phi_{\bar{\mathcal{L}}\mathcal{L}}) \sqrt{N-L} \left(\frac{1}{\|\Phi_{\bar{\mathcal{L}}\mathcal{L}}\|_1} + \frac{1}{\|\Phi_{\bar{\mathcal{L}}\mathcal{L}}\|_1} \right). \quad (15)$$

When we consider (15) in place of (8), we observe that both the algebraic and geometric methods can be viewed as attempting to minimize different parts of the same bound. MinCond aims to minimize the $\kappa(\Phi_{\bar{\mathcal{L}}\mathcal{L}})$ term in (15), while MaxMinGeo and DPP can be viewed as implicitly minimizing the $\frac{1}{\|\Phi_{\bar{\mathcal{L}}\mathcal{L}}\|_1}$ term in (15). However, according to the bound in (15), the learning error is determined not only by these terms alone, but by their combination, and further also by $\frac{1}{\|\Phi_{\bar{\mathcal{L}}\mathcal{L}}\|_1} + \frac{1}{\|\Phi_{\bar{\mathcal{L}}\mathcal{L}}\|_1}$. In our view, the entire right side of (15), which considers all of these criteria simultaneously, provides us with a more natural and reasonable criterion for manifold landmarking in the context of active learning. In particular, we can achieve manifold landmarking by solving

$$\begin{aligned} \min_{\mathcal{L}} \kappa(\Phi_{\bar{\mathcal{L}}\mathcal{L}}) \left(\frac{1}{\|\Phi_{\bar{\mathcal{L}}\mathcal{L}}\|_1} + \frac{1}{\|\Phi_{\bar{\mathcal{L}}\mathcal{L}}\|_1} \right) \\ \text{s.t. } |\mathcal{L}| = L. \end{aligned} \quad (16)$$

Here, the objective function in (16) is the right side of inequality (8). The first term $\kappa(\Phi_{\bar{\mathcal{L}}\mathcal{L}}) \frac{1}{\|\Phi_{\bar{\mathcal{L}}\mathcal{L}}\|_1}$ corresponds to a combination of algebraic and geometric manifold landmarking

methods. The second term $\kappa(\Phi_{\bar{\mathcal{L}}\bar{\mathcal{L}}}) \frac{1}{\|\Phi_{\bar{\mathcal{L}}\bar{\mathcal{L}}}\|_1}$ can be viewed as a regularizer. Specifically, $\|\Phi_{\bar{\mathcal{L}}\bar{\mathcal{L}}}\|_1 = \max_{j \in \bar{\mathcal{L}}} \sum_{i \in \bar{\mathcal{L}}} |\phi_{ij}| = \max_{j \in \bar{\mathcal{L}}} \phi_{jj} + \sum_{i \in \bar{\mathcal{L}} \setminus j} d_{ij}$, which involves the sum of distances between each unlabeled sample to the remaining unlabeled samples. This reflects the density of the samples on the manifold. By trying to minimize $\frac{1}{\|\Phi_{\bar{\mathcal{L}}\bar{\mathcal{L}}}\|_1}$, we encourage the selection of landmarks in a way that results in a set of unlabelled samples that are dense (with respect to the target manifold), which should aid in subsequent learning tasks. The importance of the regularizer is controlled by the condition number $\kappa(\Phi_{\bar{\mathcal{L}}\bar{\mathcal{L}}})$.

IV. GERSHGORIN CIRCLE-BASED LANDMARK SELECTION

A. Proposed algorithm

Optimizing (16) directly is intractable. Instead, we propose a heuristic but very effective algorithm for approximately solving the problem. In particular, our algorithm involves two key steps.

1) Constructing surrogate objective function. Given an alignment matrix Φ , we construct a regularized alignment matrix $\Psi = \Phi + \alpha \mathbf{I}_N$, where $\alpha > 0$, and replace the objective function in (16) with

$$\kappa(\Psi_{\bar{\mathcal{L}}\bar{\mathcal{L}}}) \left(\frac{1}{\|\Psi_{\bar{\mathcal{L}}\bar{\mathcal{L}}}\|_1} + \frac{1}{\|\Psi_{\bar{\mathcal{L}}\bar{\mathcal{L}}}\|_1} \right). \quad (17)$$

By replacing Φ with Ψ we can ensure that the smallest eigenvalue of Ψ is well-separated from 0, which as we will see below is key to our approach. We can make this substitution because of the following property.

Property 2. The results of the manifold learning approach in (1) or the semi-supervised manifold learning approaches in (2) and (3) are not changed by replacing Φ with Ψ .

Proof. For manifold learning, after replacing Φ with Ψ , we can rewrite the objective function in (1) as

$$\text{tr}(\mathbf{Y}\Phi\mathbf{Y}^T + \alpha\mathbf{Y}\mathbf{Y}^T).$$

Because of the normalization constraint $\mathbf{Y}\mathbf{Y}^T = \mathbf{I}_d$, we have $\text{tr}(\mathbf{Y}\mathbf{Y}^T) = \text{tr}(\mathbf{I}_d) = d$. Therefore, replacing Φ with Ψ only introduces a constant into the original objective function, which does not change the optimal point.

For the LS approach to semi-supervised manifold learning, upon replacing Φ with Ψ the objective function in (2) can be rewritten as:

$$\text{tr}(\mathbf{Z}\Phi\mathbf{Z}^T) + \alpha\text{tr}(\mathbf{Z}_{\mathcal{L}}\mathbf{Z}_{\mathcal{L}}^T) + \alpha\text{tr}(\mathbf{Z}_{\bar{\mathcal{L}}}\mathbf{Z}_{\bar{\mathcal{L}}}^T).$$

Note that $\text{tr}(\mathbf{Z}_{\bar{\mathcal{L}}}\mathbf{Z}_{\bar{\mathcal{L}}}^T) = \|\mathbf{Z}_{\bar{\mathcal{L}}}\|_F^2$. Compared with the original objective function in (2), replacing Φ with Ψ is equivalent to adding the optional regularizer of $\mathbf{Z}_{\bar{\mathcal{L}}}$ with $\gamma = \alpha$.

For the Spec method, the objective function in (3) can be rewritten as:

$$\text{tr}(\mathbf{Y}\Phi\mathbf{Y}^T) + \alpha d + \gamma\text{tr}(\mathbf{Y}_{\mathcal{L}}\mathbf{G}\mathbf{Y}_{\mathcal{L}}^T).$$

Again, replacing Φ with Ψ does not change the optimal point. \square

Following the work in [8], we can further relax (17) with the help of the Gershgorin circle theorem [9].

Theorem 1 (Gershgorin circle theorem). *For an $N \times N$ matrix Ψ with entries ψ_{ij} , its eigenvalues λ_i satisfy:*

$$|\lambda_i - \psi_{ii}| \leq r_i := \sum_{j \neq i} |\psi_{ij}|$$

for $i = 1, \dots, N$. Defining $c_i := \psi_{ii}$, the set $\mathcal{C}_i = \{x : |x - c_i| \leq r_i\}$ is called the i^{th} Gershgorin circle of Ψ , where C_i is the center and r_i is the radius of the circle.

Denote the center and the radius of Ψ 's i^{th} Gershgorin circle as $c_i = \psi_{ii}$ and $r_i = \sum_{j \neq i} |\psi_{ij}|$, respectively, and denote the radius of $\Psi_{\bar{\mathcal{L}}\bar{\mathcal{L}}}$'s i^{th} Gershgorin circle as $s_i = \sum_{j \in \bar{\mathcal{L}} \setminus i} |\psi_{ij}|$. From Theorem 1 and the fact that Ψ is symmetric, the eigenvalues of Ψ (and its arbitrary principal submatrix) are real and must fall within $\cup_i [c_i - r_i, c_i + r_i]$. Moreover, we can always choose an $\alpha > 0$ such that the lower bound $\min(c_i - r_i)$ is positive. In such a situation, we obtain an upper bound for the condition number of Ψ :

$$\kappa(\Psi) = \left| \frac{\lambda_{\max}(\Psi)}{\lambda_{\min}(\Psi)} \right| \leq \frac{\max(c_i + r_i)}{\min(c_i - r_i)}. \quad (18)$$

Moreover, note that $\|\Psi\|_1 = \max_{1 \leq j \leq N} \sum_{i=1}^N |\psi_{ij}| = \max_{1 \leq j \leq N} |c_j + r_j|$. Similarly, we have $\|\Psi_{\bar{\mathcal{L}}\bar{\mathcal{L}}}\|_1 = \max_{i \in \bar{\mathcal{L}}} (c_i + s_i)$ and $\|\Psi_{\bar{\mathcal{L}}\bar{\mathcal{L}}}\|_1 = \max_{i \in \bar{\mathcal{L}}} (r_i - s_i)$. If we define $\Psi_{\bar{\mathcal{L}}} = [\Psi_{\bar{\mathcal{L}}\mathcal{L}}, \Psi_{\bar{\mathcal{L}}\bar{\mathcal{L}}}]$, then we also have $\|\Psi_{\bar{\mathcal{L}}}\|_1 = \max_{i \in \bar{\mathcal{L}}} (c_i + r_i)$. Therefore, we have

$$\begin{aligned} & \kappa(\Psi_{\bar{\mathcal{L}}\bar{\mathcal{L}}}) \left(\frac{1}{\|\Psi_{\bar{\mathcal{L}}\bar{\mathcal{L}}}\|_1} + \frac{1}{\|\Psi_{\bar{\mathcal{L}}\bar{\mathcal{L}}}\|_1} \right) \\ & \leq \frac{\max_{i \in \bar{\mathcal{L}}} (c_i + s_i)}{\min_{i \in \bar{\mathcal{L}}} (c_i - s_i)} \left(\frac{\|\Psi_{\bar{\mathcal{L}}\bar{\mathcal{L}}}\|_1 + \|\Psi_{\bar{\mathcal{L}}\bar{\mathcal{L}}}\|_1}{\|\Psi_{\bar{\mathcal{L}}\bar{\mathcal{L}}}\|_1 \|\Psi_{\bar{\mathcal{L}}\bar{\mathcal{L}}}\|_1} \right) \\ & \leq \frac{\max_{i \in \bar{\mathcal{L}}} (c_i + s_i)}{\min_{i \in \bar{\mathcal{L}}} (c_i - s_i)} \frac{2\|\Psi_{\bar{\mathcal{L}}}\|_1}{\|\Psi_{\bar{\mathcal{L}}\bar{\mathcal{L}}}\|_1 \|\Psi_{\bar{\mathcal{L}}\bar{\mathcal{L}}}\|_1} \\ & = \frac{\max_{i \in \bar{\mathcal{L}}} (c_i + s_i)}{\min_{i \in \bar{\mathcal{L}}} (c_i - s_i)} \frac{2 \max_{i \in \bar{\mathcal{L}}} (c_i + r_i)}{\max_{i \in \bar{\mathcal{L}}} (r_i - s_i) \max_{i \in \bar{\mathcal{L}}} (c_i + s_i)} \\ & = \frac{2 \max_{i \in \bar{\mathcal{L}}} (c_i + r_i)}{\min_{i \in \bar{\mathcal{L}}} (c_i - s_i) \max_{i \in \bar{\mathcal{L}}} (r_i - s_i)} \\ & = Q(\bar{\mathcal{L}}). \end{aligned}$$

The second inequality is based on the fact that

$$\begin{aligned} \|\Psi_{\bar{\mathcal{L}}\bar{\mathcal{L}}}\|_1 + \|\Psi_{\bar{\mathcal{L}}\bar{\mathcal{L}}}\|_1 & \leq 2 \max\{\|\Psi_{\bar{\mathcal{L}}\bar{\mathcal{L}}}\|_1 + \|\Psi_{\bar{\mathcal{L}}\bar{\mathcal{L}}}\|_1\} \\ & = 2\|\Psi_{\bar{\mathcal{L}}}\|_1. \end{aligned} \quad (19)$$

$Q(\bar{\mathcal{L}})$ gives an upper bound for our error that can be used as a surrogate for our objective function in (16).¹

2) Deleting and updating Gershgorin circles. The second key step of our algorithm is deleting and updating Gershgorin circles iteratively, such that in each step, the surrogate function is reduced in a greedy fashion. Specifically, we propose our

¹We note that there is an alternative derivation which results in the exact same function $Q(\bar{\mathcal{L}})$ as an upper bound on the learning error. In particular, if one begins in (8) by establishing a bound on the learning error in the ℓ_1 norm, then one can obtain a similar bound by bounding κ_1 using the fact that for any $N \times N$ matrix \mathbf{A} , $\|\mathbf{A}^{-1}\|_1 \leq N / \min_i |a_{ii}| - r_i(\mathbf{A})$, where r_i is defined as above. This is a consequence of standard norm inequalities combined with the Ahlberg-Nilson-Varah [50], [51] bound on $\|\mathbf{A}^{-1}\|_\infty$.

Algorithm 2 Gershgorin Circle-based Landmark Selection (GCLS)**Input:** $\Phi = [\phi_{ij}] \in \mathbb{R}^{N \times N}$, the number of landmarks L .**Output:** A set of landmarks \mathcal{L} .

```

1: Initialize  $\mathcal{L} = \emptyset$ ,  $\bar{\mathcal{L}} = \{1, \dots, N\}$ .
2: Compute the bound of  $\lambda(\Phi)$ :  $b_{\min}$ ,  $b_{\max}$ .
3: Set  $\alpha = \max\{0, -b_{\min}\}$ , construct  $\Psi = \Phi + \alpha I_N$ .
4: for  $i = 1 : N$  do
5:   Initialize  $c_i = \psi_{ii}$ ,  $r_i = \sum_{j \neq i} |\psi_{ij}|$ ,  $s_i = r_i$ .
6: end for
7: for  $l = 1 : L$  do
8:   Select landmark:  $\hat{i} = \arg \min_{i \in \bar{\mathcal{L}}} Q(\bar{\mathcal{L}} \setminus i)$ .
9:    $\mathcal{L} = \mathcal{L} \cup \hat{i}$ ,  $\bar{\mathcal{L}} = \bar{\mathcal{L}} \setminus \hat{i}$ .
10:  for  $i \in \bar{\mathcal{L}}$  do
11:    Update  $s_i = s_i - \psi_{i\hat{i}}$ .
12:  end for
13: end for

```

Gershgorin circle-based landmark selection (**GCLS**) algorithm in Algorithm 2. The configuration of α ensures that b_{\min} is nonnegative. After initialization, we select landmarks by deleting Gershgorin circles (i.e., the rows/columns of Ψ) iteratively (Line 7-13). At each iteration, the deleted circle must reduce the value of the surrogate function Q as much as possible (line 8). This process is then repeated. As a result, we shrink an upper bound of (17) and thereby hope to obtain a good approximation to the solution of (16).

B. Further analysis and comparisons

Compared with existing methods like MaxMinGeo, DPP, and MinCond, our GCLS method has several advantages. We summarize our comparison of these algorithms in Table I.

- **Universality with respect to alignment matrix.** Both MaxMinGeo and DPP require the alignment matrix to be a graph Laplacian matrix because they need to compute the geodesic (or pairwise) distance between samples. For MinCond, the eigenvalues of the alignment matrix must lie in the interval $(0, 2)$ because the logarithm of the alignment matrix is calculated in each step. A contribution of our GCLS method is adding a pre-processing step to construct a well-conditioned alignment matrix, and proving that it does not change the ultimate result of semi-supervised manifold learning. With the help of this pre-processing step, our algorithm can be used with arbitrary alignment matrices.
- **Complexity and scalability.** All four of these methods select L landmarks from N samples. The space complexity of these algorithms is $\mathcal{O}(N)$ for storing the sparse alignment matrix defined on a K -NN graph. The time complexity of these algorithms differ substantially. The time complexity of MaxMinGeo is $\mathcal{O}(LN \log(N))$ because the shortest path algorithm is applied to compute the geodesic distance between samples. The time complexity of DPP is $\mathcal{O}(KL)$, where K is the number of neighbors for the samples in the K -NN graph, because DPP only takes advantage of the pairwise distance be-

TABLE I: Comparisons for various algorithms.

Algorithm	Φ	Obj. function	Complexity
MaxMinGeo	Laplacian	$\max \min d_{ij}$	$\mathcal{O}(LN \log(N))$
DPP	Laplacian	$\text{approx. } \max \min d_{ij}$	$\mathcal{O}(KL)$
MinCond	$\lambda \in (0, 2)$	$\min \kappa(\Phi_{\bar{\mathcal{L}}\bar{\mathcal{L}}})$	$\mathcal{O}(LN^3)$
GCLS	Arbitrary	$\min \frac{\kappa(\Psi_{\bar{\mathcal{L}}\bar{\mathcal{L}}})}{\ \Psi_{\bar{\mathcal{L}}\bar{\mathcal{L}}}\ _1} + \frac{\kappa(\Psi_{\bar{\mathcal{L}}\bar{\mathcal{L}}})}{\ \Psi_{\bar{\mathcal{L}}\bar{\mathcal{L}}}\ _1}$	$\mathcal{O}(NL)$

tween samples and their neighbors in each step. The time complexity of MinCond is $\mathcal{O}(LN^3)$ because MinCond computes the logarithm of the alignment matrix in each step. Finally, the time complexity of our GCLS algorithm is $\mathcal{O}(NL)$. The time complexity of our algorithm is only higher than that of DPP, which has good scalability for real-time and large-scale applications.

C. Summary

Our GCLS method can be viewed as a generalization of existing methods, which is robust to various alignment matrices and has relatively low complexity. It should be noted that like existing methods, our heuristic method can only obtain a suboptimal landmarking solution. However, experimental results in the following section will show that our method performs well in practical situations.

V. EXPERIMENTS

We compare our GCLS algorithm with existing landmarking algorithms (random selection, MaxMinGeo [41], DPP [43], and MinCond [8]) on multiple data sets. For each data set, we test the algorithms with 20 trials and record the averaged results. In each trial, we first select N samples randomly and construct a K -NN graph. Then, we select L landmarks via each landmarking algorithm and learn labels for the remaining samples via semi-supervised manifold learning methods. Using noisy data (Gaussian noise with zero mean and variance $\sigma^2 = 0.01$), we test the robustness of each algorithm. In regression tasks, the relative learning error is calculated as

$$E = \frac{\|\hat{\mathbf{Z}}_u - \mathbf{Z}_u\|_F}{\|\mathbf{Z}_u\|_F} \times 100\%.$$

In classification tasks, the classification accuracy is recorded. The runtime of the algorithm and the bound on the learning error of $\kappa(\Psi_{\bar{\mathcal{L}}\bar{\mathcal{L}}}) \left(\frac{1}{\|\Psi_{\bar{\mathcal{L}}\bar{\mathcal{L}}}\|_1} + \frac{1}{\|\Psi_{\bar{\mathcal{L}}\bar{\mathcal{L}}}\|_1} \right)$ are also recorded.

In regression tasks, the semi-supervised manifold learning algorithm used in our work is the LS algorithm in [2], i.e., the optimization problem in (2). In classification tasks, a classifier based on the label-consistent K-SVD (LCKSVD) [52] is applied. The parameters of various landmark selection algorithms are set as follows. For MaxMinGeo, the number of initial landmarks are 3 random ones. For DPP, we sample the point \mathbf{x}_i as the new landmark with a probability $p_i \propto \prod_j (1 - g_D(\mathbf{x}_i - \mathbf{x}_j))$, where \mathbf{x}_j is the j^{th} existing landmark and the function $g_D(\mathbf{x}) = \exp(-\|\mathbf{x}\|_2^2 / 2D^2)$. The bandwidth D is equal to the dimension of sample space. Different K 's are used to construct the K -NN graph for each data set. MaxMinGeo and DPP use the graph Laplacian as the alignment matrix while the remaining methods use the LTSA-based alignment

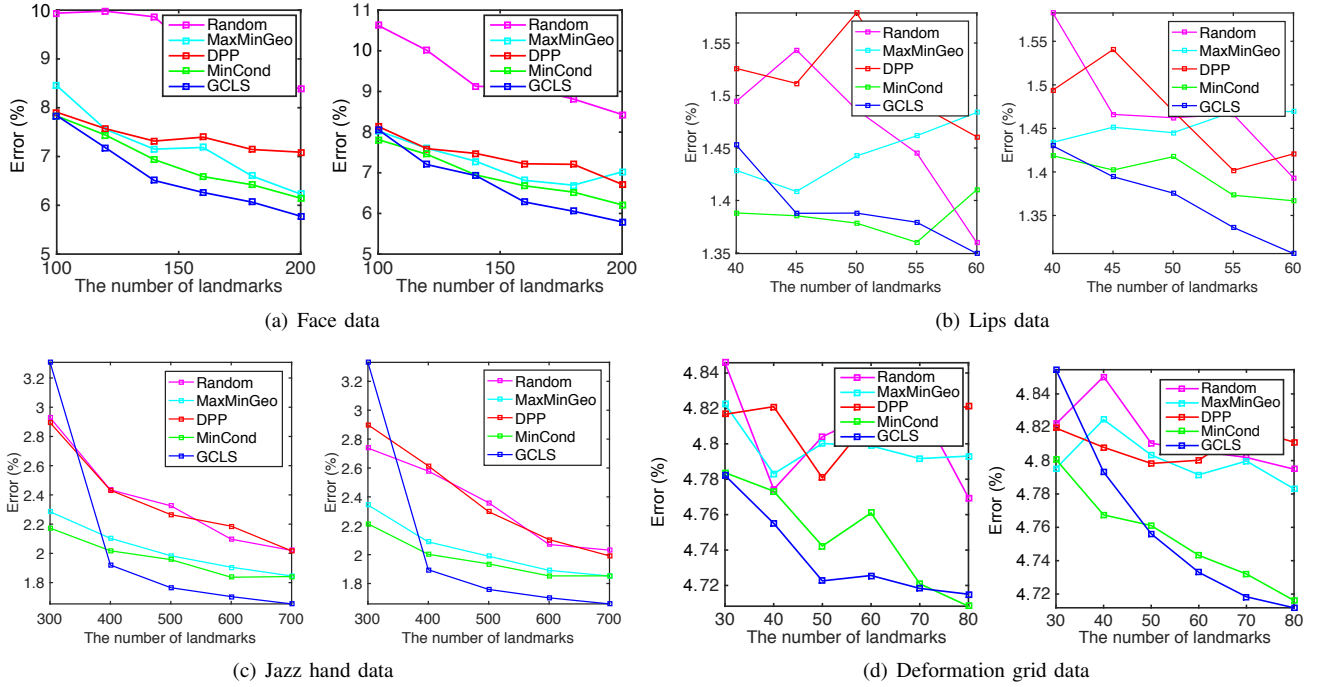


Fig. 1: The relative estimation errors obtained by our methods on various data sets are shown. In each subfigure, the right one shows the results on clear data set and the left one shows the results on noisy data set.

matrix. All the SSML methods use the LTSA-based alignment matrix, as does the computation of the error bound.

A. Regression tasks

We test the different landmarking methods on four data sets, including the face data set from [22], the lips and the Jazz hand data sets from [53], and the deformed grid data set from [54]. For each data set, we select N samples randomly and landmark L of them in each trial.

- For the face data set, $N = 500$ face images (with size 64×64) are selected randomly, where the labels include a lighting intensity and two pose parameters ($d = 3$). We apply Principal Component Analysis (PCA) to reduce the dimension of data to $D = 200$, and then, we construct a K -NN graph with $K = 30$ based on the samples obtained by PCA. For each landmark selection algorithm, we select $L = [100, \dots, 200]$ landmarks respectively and then learn the labels for the remaining samples directly.
- For the lips data set, $N = 80$ lip images (with size 40×45) are selected randomly, where the labels include four key points indicating the deformation of mouth ($d = 8$). We apply PCA to obtain the samples with $D = 196$ and construct a K -NN graph with $K = 35$. For each landmark selection algorithm, we select $L = [40, \dots, 60]$ landmarks respectively and then learn the labels for the remaining samples directly.
- For the Jazz hand data set, $N = 1000$ hand motion images (with size 66×88 , $D = 5808$) are selected randomly, whose labels include four key points indicating the motion of two arms ($d = 8$). Similarly, we apply PCA to obtain the samples with $D = 498$ and a K -NN graph

with $K = 30$. For each landmark selection algorithm, we select $L = [300, \dots, 700]$ landmarks respectively and then learn the labels for the remaining samples directly.

- For the deformed grid data set, a reference grid image is given in Fig. 2(d), whose key points are shown as red crosses. Using various operations of deformation, a set of deformed images is generated. We aim to label a small number of key points in these images and estimate the locations of the remaining key points. Specifically, we segment each image into 25 patches (with size 22×22 , $D = 484$), each of which contains 4 key points ($d = 8$), as Fig. 2(d) shows. In each trial, we randomly select $N = 400$ patches from the deformed images and then construct a K -NN graph with $K = 30$. For each landmark selection algorithm, we select $L = [30, \dots, 80]$ landmarks and then learn labels for the remaining samples directly.

The comparisons for various methods is shown in Fig. 1 and Table II. In most situations, our GCLS algorithm achieves lower learning error than its competitors with respect to various choices of L . In particular, for the face data set, our GCLS is superior to its competitors when testing on both clean and noisy data. For the lips data set, the performance of our GCLS is comparable to that of MinCond when testing on clean data. However, when it comes to noisy data, the superiority of our GCLS is obvious. This suggests that our method is more robust to the noise in the data. For the Jazz hand data set, while our GCLS performs worse than others when L is small, its error reduces quickly when L increases. For the deformed grid data set, our GCLS method outperforms its competitors in clean data. When testing on noisy data, the estimation error obtained by our GCLS converges quickly when L increases.

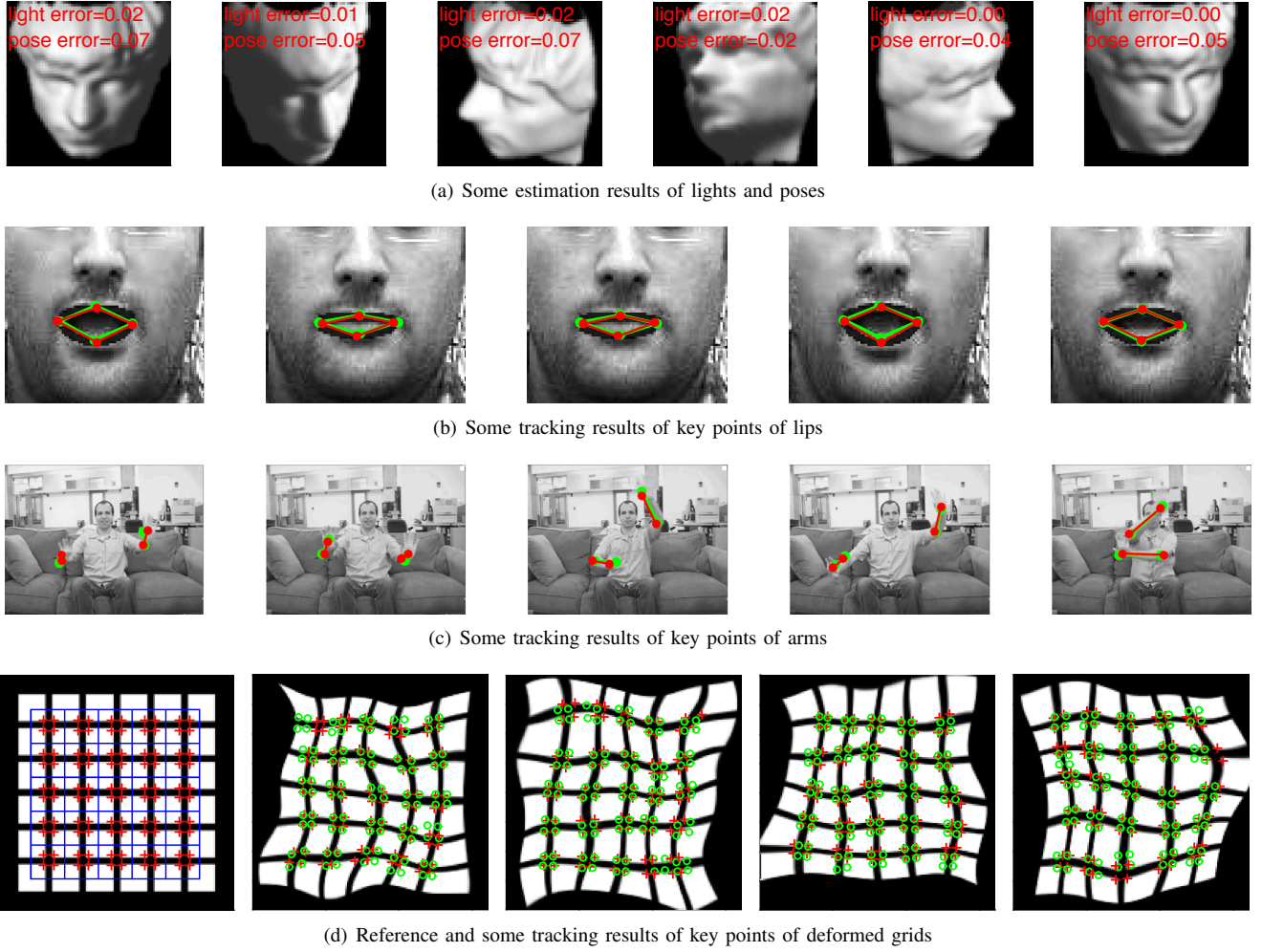


Fig. 2: The regression results of our method on various data sets are visualized. In subfigure (a), the relative estimation errors are labeled as red. In subfigures (b,c), the real and estimated key points are labeled as green and red, respectively. In subfigure (d), the segmentation of reference grid (blue lines) and key points (red crosses). In each deformed image, estimated locations of key points (green circles) and ground truth (red crosses) are given.

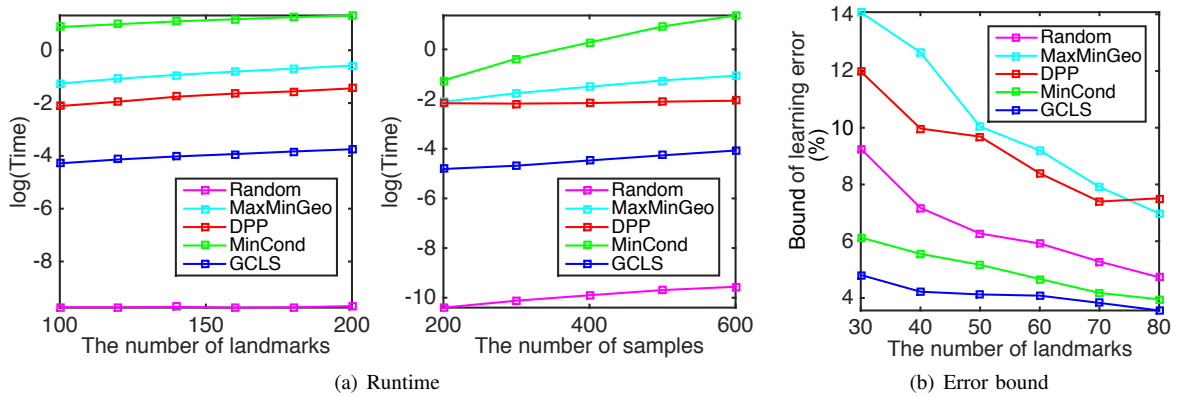


Fig. 3: (a) The run time versus the number of landmarks L ($N = 500$) and the number of samples N ($L = 100$) respectively. (b) Comparison of the value of the objective function in (16).

Additionally, the numerical comparisons for various methods on clean data sets are listed in Table II. In summary, when just landmarking a few samples, our method is at least comparable

to other methods. As the number of landmarks increases, the superiority of our method becomes more and more obvious.

The runtime of each algorithm is given in Fig. 3(a).

TABLE II: Comparisons for various methods on learning errors (%).

Data	L	Random	MaxMinGeo	DPP	MinCond	GCLS
Face $N = 500$	140	9.86	7.15	7.32	6.94	6.51
	160	8.99	7.19	7.40	6.59	6.26
	180	8.75	6.60	7.14	6.42	6.15
	200	8.38	6.23	7.09	6.15	5.78
Lips $N = 80$	45	1.54	1.41	1.51	1.38	1.37
	50	1.49	1.44	1.59	1.38	1.39
	55	1.45	1.46	1.49	1.36	1.38
	60	1.36	1.48	1.46	1.41	1.35
Jazz Hand $N = 1000$	300	2.93	2.29	2.89	2.17	3.31
	400	2.43	2.10	2.43	2.02	1.92
	500	2.33	1.98	2.27	1.96	1.77
	600	2.10	1.91	2.19	1.84	1.70
Grid $N = 400$	700	2.02	1.85	2.02	1.84	1.65
	30	4.85	4.82	4.81	4.78	4.78
	40	4.77	4.78	4.82	4.77	4.75
	50	4.80	4.80	4.78	4.74	4.72
	60	4.82	4.79	4.81	4.76	4.73

TABLE III: Classification accuracy (%).

Data set	AR Face			Extended YaleB		
	10/Class	15/Class	20/Class	15/Class	20/Class	25/Class
Random	82.00	85.50	87.67	74.62	79.05	93.16
MaxMinGeo	85.00	87.33	89.17	75.30	83.73	93.22
DPP	80.67	84.00	87.17	72.95	81.05	89.15
MinCond	86.67	87.00	89.00	74.46	83.89	93.91
GCLS	86.67	88.67	89.67	75.96	84.97	94.22

Consistent with our analysis, the speed of our algorithm is competitive and achieves a balance between complexity and performance. Note that although the results of MinCond are close to (though still worse than) ours, its run time is about 100 times longer. Note also that although the complexity of DPP is lower than ours, our algorithm obtains significantly lower error than DPP. Finally, in Fig.3(b) we compare the error bound which serves as the objective function in (16) versus L for the different algorithms. As expected, GCLS obtains a much tighter bound than others.

B. Classification tasks

We also apply our landmarking algorithm to the classification tasks of the AR-face and the Extended YaleB data sets, respectively. We use a subset of the AR-face data set [55] consisting of 2600 images from 100 subjects. The Extended YaleB contains 2414 frontal face images of 38 persons. After selecting labeled samples via the different landmarking algorithms, we apply the LCKSVD algorithm in [52] to a learn dictionary and attain sparse codes for the samples. The size of the dictionary and the parameters of the learning algorithm follow the setting in [52]. Finally, taking the learned sparse codes as the features of the samples, we train an SVM classifier [56]. Table III compares classification results corresponding to various algorithms. We observe that GCLS significantly improves classification accuracy, especially in the case of very few landmarks.

VI. CONCLUSION

In this paper, we study the active manifold learning problem and propose a landmark selection algorithm based on the

Gershgorin circle theorem. We establish connections among various landmark selection algorithms and propose a unified algorithmic framework. Compared with other competitors, our GCLS algorithm has lower complexity and higher performance in both regression and classification tasks.

APPENDIX

A. A review of manifold learning

Let $\mathbf{X} = [\mathbf{x}_1, \dots, \mathbf{x}_N] \in \mathbb{R}^{D \times N}$ be a set of samples from a manifold \mathcal{X} . Let $\mathbf{y}_i \in \mathbb{R}^d$ ($d \ll D$) represent the unknown low-dimensional parameter vector corresponding to \mathbf{x}_i . We can build a graph for the samples as follows: for each sample \mathbf{x}_i , its K nearest neighbors are selected and denoted as $\mathbf{X}_i \in \mathbb{R}^{D \times K}$. This graph provides us with a significant amount of geometrical information about the manifold. We can then solve the manifold learning problem via several different strategies.

- **LLE** characterizes the local geometry of the manifold by finding linear coefficients that reconstruct each sample from its neighbors [20]. The coefficients can be learned by minimizing the reconstruction error. The coefficients preserve the relationships among the samples and their neighbors, which are assumed to be inherited by the low-dimensional parameters. Formally, we first compute coefficients by

$$\begin{aligned} \min_{\mathbf{W}} \quad & \sum_{i=1}^N \|\mathbf{x}_i - \mathbf{X}_i \mathbf{w}_i\|_2^2 \\ \text{s.t.} \quad & \sum_{j=1}^K w_{ij} = 1, \end{aligned} \quad (20)$$

where $\mathbf{W} = [\mathbf{w}_1, \dots, \mathbf{w}_N]$, $\mathbf{w}_i = [w_{i1}, \dots, w_{iK}]^T$. Then, $\mathbf{Y} = [\mathbf{y}_1, \dots, \mathbf{y}_N]$ is computed by

$$\min_{\mathbf{Y}} \sum_{i=1}^N \|\mathbf{y}_i - \mathbf{Y}_i \mathbf{w}_i\|_2^2 = \min_{\mathbf{Y}} \text{tr}(\mathbf{Y} \mathbf{\Phi} \mathbf{Y}^T), \quad (21)$$

where $\mathbf{Y}_i = [\mathbf{y}_{i1}, \dots, \mathbf{y}_{iK}]$ contains the neighbors of \mathbf{y}_i , whose columns are the K nearest samples of \mathbf{y}_i . The entries of $\mathbf{\Phi}$ are given by $\phi_{ij} = \delta_{ij} - w_{ij} - w_{ji} + \mathbf{w}_i^T \mathbf{w}_j$, $i, j = 1, \dots, N$, where δ_{ij} is 1 if $i = j$ and 0 otherwise. We add constraints $\sum_i \mathbf{y}_i = \mathbf{0}$ and $\mathbf{Y} \mathbf{Y}^T = \mathbf{I}_d$ to fix the scaling, translation, and rotation of the latent variables. The resulting problem reduces to finding the smallest $d+1$ eigenvectors of $\mathbf{\Phi}$.

- **LTSA** also tries to capture the local geometry of \mathcal{X} [21]. Assume that there exists a mapping from the latent space to the ambient space, i.e., $f: \mathcal{Y} \mapsto \mathcal{X}$. Instead of directly computing reconstruction coefficients, LTSA approximates the tangent space at each sample. According to the Taylor expansion, for each $\mathbf{x}_i \in \mathbf{X}_i$ we have

$$\mathbf{x}_i - \mathbf{x}_j \approx \mathbf{J}_i(\mathbf{y}_i - \mathbf{y}_j) = \mathbf{J}_i \boldsymbol{\theta}_j^i. \quad (22)$$

Here $\mathbf{J}_i = [\frac{\partial f}{\partial \mathbf{y}_i}] \in \mathbb{R}^{D \times d}$ is the Jacobian matrix of f at \mathbf{y}_i , which can be calculated as the singular vectors corresponding to the largest d singular values of $\mathbf{X}_i - \mathbf{x}_i \mathbf{e}^T$, $\mathbf{e} = [1, \dots, 1]^T$. Then $\boldsymbol{\Theta}_i = [\boldsymbol{\theta}_1^i, \dots, \boldsymbol{\theta}_K^i] \in \mathbb{R}^{d \times K}$ are local coordinates of \mathbf{X}_i in the tangent space. After computing the local tangent space at each sample, the global coordinates \mathbf{Y} are computed by aligning the local tangent spaces together. Assuming that the corresponding

global parameter vectors \mathbf{Y}_i differ from the local ones Θ_i by a local affine transformation, we minimize the errors of the transformation by $\min_{\Phi_i} \|\mathbf{Y}_i \Phi_i\|_F^2$, where Φ_i is the orthogonal projection whose null space is spanned by the columns of $[\mathbf{1}, \Theta_i]$. In practice, we obtain \mathbf{Y} by

$$\min_{\mathbf{Y}} \sum_{i=1}^N \|\mathbf{Y}_i \Phi_i\|_F^2 = \min_{\mathbf{Y}} \text{tr}(\mathbf{Y} \Phi \mathbf{Y}^T). \quad (23)$$

Here $\Phi = \sum_{i=1}^N \mathbf{S}_i \Phi_i \mathbf{S}_i^T$, where the \mathbf{S}_i are 0-1 selection matrices ensuring $\mathbf{Y}_i = \mathbf{Y} \mathbf{S}_i$. Adding the normalization conditions $\mathbf{Y} \mathbf{Y}^T = \mathbf{I}_d$ and $\mathbf{Y} \mathbf{1} = \mathbf{0}$, the solution of (23) is the set of eigenvectors corresponding to the 2nd to $(d+1)$ th smallest eigenvalues of Φ . In recent years, LTSA has been extended to more complicated parametric models [57], achieving encouraging results in many applications [58], [59].

- **ISOMAP** seeks an embedding preserving the geodesic distance between samples [22]. The geodesic distances are computed by finding the shortest paths in the graph connecting neighboring data points. Let \mathbf{D} denote the matrix of squared geodesic distances. Let $\mathbf{P} \in \mathbb{R}^{N \times N}$ denote the projection matrix $\mathbf{I}_N - \frac{1}{N} \mathbf{e} \mathbf{e}^T / N$. The low dimensional global coordinates are computed by finding the eigenvectors corresponding to the d maximum eigenvalues of $\mathbf{A} = -\frac{1}{2} \mathbf{P}^T \mathbf{D} \mathbf{P}$. According to [2], the ISOMAP problem can also be rewritten as follows: Let $\mathbf{Q} \mathbf{\Lambda} \mathbf{Q}^T$ be the eigen-decomposition of \mathbf{A} . $\mathbf{Q} = [\mathbf{q}_1, \dots, \mathbf{q}_N]$ and $\mathbf{\Lambda} = \text{diag}(\lambda_1, \dots, \lambda_N)$, $\lambda_1 \geq \lambda_2 \geq \dots \geq \lambda_N$. Then we compute the alignment matrix as

$$\Phi = \lambda_1 \mathbf{I}_N - \mathbf{A} - \sum_{i=2}^d (\lambda_1 - \lambda_i) \mathbf{q}_i \mathbf{q}_i^T - \frac{\lambda_1}{N} \mathbf{e} \mathbf{e}^T, \quad (24)$$

where Φ has $d+1$ zero eigenvalues and its null space is spanned by $[\mathbf{q}_1, \dots, \mathbf{q}_d, \mathbf{e}]$. Therefore we can solve the ISOMAP problem via $\min_{\mathbf{Y}} \text{tr}(\mathbf{Y} \Phi \mathbf{Y}^T)$ as well.

As shown above, although the three algorithms compute the alignment matrix Φ from different points of view, they all reduce to the same eigen-problem.

B. Theoretical bound of condition number of submatrix

Mathematically, given an $N \times N$ matrix \mathbf{B} with singular values $\sigma_1(\mathbf{B}) \geq \sigma_2(\mathbf{B}) \geq \dots \geq \sigma_N(\mathbf{B}) \geq 0$, if there is a gap between $\sigma_n(\mathbf{B})$ and $\sigma_{n+1}(\mathbf{B})$, and $\sigma_{n+1}(\mathbf{B})$ is sufficiently small, one may assume that \mathbf{B} has a numerical rank n . In this case, RRQR-factorization attempts to find a permutation matrix Π such that the QR factorization

$$\begin{aligned} \mathbf{B} \Pi &= \mathbf{Q} \mathbf{R}, \\ \mathbf{R} &= \begin{bmatrix} \mathbf{R}_{11} & \mathbf{R}_{12} \\ \mathbf{0} & \mathbf{R}_{22} \end{bmatrix}, \end{aligned} \quad (25)$$

satisfies that $\mathbf{R}_{11} \in \mathbb{R}^{n \times n}$ and \mathbf{R}_{11} 's smallest singular value $\sigma_{\min}(\mathbf{R}_{11}) \approx \sigma_n(\mathbf{B})$ and \mathbf{R}_{22} 's largest singular value $\sigma_{\max}(\mathbf{R}_{22}) \approx \sigma_{n+1}(\mathbf{B})$, where \mathbf{Q} is orthogonal and \mathbf{R} is upper triangular. In essence, \mathbf{R}_{11} captures the well-conditioned part of \mathbf{B} . Readers can refer to [49] for the details of RRQR.

An important property of RRQR is that there exists an RRQR such that

$$\sigma_{\min}(\mathbf{R}_{11}) \geq \frac{\sigma_n(\mathbf{B})}{\sqrt{n(N-n)+1}}. \quad (26)$$

Making use of this property, we obtain an upper bound for the condition number of a principal submatrix of Φ .

Theorem 2. *Let the eigenvalues of Φ be $\lambda_1(\Phi) \geq \lambda_2(\Phi) \geq \dots \geq \lambda_N(\Phi) \geq 0$. There exists an $(N-L) \times (N-L)$ principal submatrix Φ_{22} of Φ such that*

$$\kappa(\Phi_{22}) \leq [L(N-L)+1] \frac{\lambda_1(\Phi)}{\lambda_{N-L}(\Phi)}. \quad (27)$$

Proof. Since Φ is positive semidefinite, there is an $N \times N$ \mathbf{B} such that $\Phi = \mathbf{B}^T \mathbf{B}$. Let \mathbf{B} have an RRQR (25) satisfying (26) with $n = N-L$. Now notice

$$\begin{aligned} \Pi^T \Phi \Pi &= (\mathbf{B} \Pi)^T (\mathbf{B} \Pi) \\ &= \mathbf{R}^T \mathbf{R} \\ &= \begin{bmatrix} \mathbf{R}_{11}^T \mathbf{R}_{11} & \mathbf{R}_{12}^T \mathbf{R}_{12} \\ \mathbf{R}_{12}^T \mathbf{R}_{12} & \mathbf{R}_{12}^T \mathbf{R}_{12} + \mathbf{R}_{22}^T \mathbf{R}_{22} \end{bmatrix} \end{aligned} \quad (28)$$

to see that Φ has an $(N-L) \times (N-L)$ principle submatrix $\Phi_{22} = \mathbf{R}_{11}^T \mathbf{R}_{11}$ whose smallest eigenvalue is

$$\begin{aligned} \sigma_{\min}(\mathbf{R}_{11})^2 &\geq \left[\frac{\sigma_{N-L}(\mathbf{B})}{\sqrt{L(N-L)+1}} \right]^2 \\ &= \frac{\lambda_{N-L}(\Phi)}{L(N-L)+1}, \end{aligned} \quad (29)$$

because $\lambda_{N-L}(\Phi) = [\sigma_{N-L}(\mathbf{B})]^2$. The result follows by noting that $\lambda_{\max}(\Phi_{22}) \leq \lambda_1(\Phi)$. \square

C. Proof of Property 1

The alignment matrix $\Phi = [\phi_{ij}]$ in (1, 2, 3) is defined on the K -NN graph, which can be generated by various manifold learning methods, including LE [23], LLE [20] and LTSA [21].

- **LE** uses a Laplacian graph matrix as the alignment matrix. Suppose that d_{ij} is the distance between sample \mathbf{x}_i and its neighbor \mathbf{x}_j . $\phi_{ij} = -d_{ij}$ if \mathbf{x}_i and \mathbf{x}_j are neighbors, otherwise $\phi_{ij} = 0$, and $\phi_{ii} = \sum_j d_{ij}$.
- **LLE** reconstructs the local geometry of the manifold by self-representation. The entries of Φ are given by

$$\phi_{ij} = \delta_{ij} - w_{ij} - w_{ji} + \mathbf{w}_i^T \mathbf{w}_j, \quad i, j = 1, \dots, N.$$

- **LTSA** approximates the local tangent space of each sample by Taylor expansion (22). The matrix $\Theta_i = [\theta_1^i, \dots, \theta_K^i] \in \mathbb{R}^{d \times K}$ are local latent variables of \mathbf{X}_i in the tangent space. Assuming that there exists an affine transformation between the global latent variables \mathbf{Y}_i and the local ones Θ_i , we minimize the errors of the transformation by

$$\min_{\mathbf{B}_i} \|\mathbf{Y}_i \mathbf{B}_i\|_F^2,$$

where \mathbf{B}_i is the orthogonal projection whose null space is spanned by the columns of $[\mathbf{1}, \Theta_i]$. Therefore, the

alignment matrix $\Phi = \sum_{i=1}^N \mathbf{S}_i \mathbf{B}_i \mathbf{B}_i^T \mathbf{S}_i^T$, where \mathbf{S}_i are 0-1 selection matrix ensuring $\mathbf{X}_i = \mathbf{X} \mathbf{S}_i$.

Therefore, for the alignment matrix generated by these methods, only the elements corresponding to neighboring samples are nonzero.

ACKNOWLEDGMENT

This work is supported in part by NSF grants DMS-1317424, and CCF-1350616, and AFOSR grant FA9550-14-1-0342, as well as a gift from the Alfred P. Sloan Foundation.

REFERENCES

- [1] M. Belkin, P. Niyogi, and V. Sindhwani, "Manifold regularization: A geometric framework for learning from labeled and unlabeled examples," *J. Mach. Learn. Res.*, vol. 7, pp. 2399–2434, 2006.
- [2] X. Yang, H. Fu, H. Zha, and J. Barlow, "Semi-supervised nonlinear dimensionality reduction," in *Proc. Int. Conf. Mach. Learn. (ICML)*, 2006, pp. 1065–1072.
- [3] Z. Zhang, H. Zha, and M. Zhang, "Spectral methods for semi-supervised manifold learning," in *Proc. IEEE Conf. Comp. Vision and Pattern Recognition (CVPR)*, 2008, pp. 1–6.
- [4] M. Zheng, J. Bu, C. Chen, C. Wang, L. Zhang, G. Qiu, and D. Cai, "Graph regularized sparse coding for image representation," *IEEE Trans. Image Process.*, vol. 20, no. 5, pp. 1327–1336, 2011.
- [5] M. Belkin and P. Niyogi, "Semi-supervised learning on Riemannian manifolds," *Mach. Learn.*, vol. 56, pp. 209–239, 2004.
- [6] H. Xu, L. Yu, D. Luo, H. Zha, and Y. Xu, "Dictionary learning with mutually reinforcing group-graph structures," in *Proc. AAAI Conf. Artificial Intell. (AAAI)*, 2015, pp. 3101–3107.
- [7] X. Zhu, J. Lafferty, and Z. Ghahramani, "Combining active learning and semi-supervised learning using Gaussian fields and harmonic functions," in *Proc. ICML Work. on the Continuum from Labeled to Unlabeled Data in Machine Learning and Data Mining*, 2003, pp. 58–65.
- [8] H. Xu, H. Zha, R.-C. Li, and M. Davenport, "Active manifold learning via Gershgorin circle guided sample selection," in *Proc. AAAI Conf. Artificial Intell. (AAAI)*, 2015, pp. 3108–3114.
- [9] S. Geršgorin, "Über die abgrenzung der eigenwerte einer matrix," *Izv. Akad. Nauk. USSR Otd. Fiz.-Mat. Nauk*, no. 6, pp. 749–754, 1931.
- [10] D. Donoho and C. Grimes, "Image manifolds which are isometric to Euclidean space," *J. Math. Imag. and Vision*, vol. 23, no. 1, pp. 5–24, 2005.
- [11] K. Weinberger and L. Saul, "Unsupervised learning of image manifolds by semidefinite programming," *Int. J. Comp. Vision*, vol. 70, no. 1, pp. 77–90, 2006.
- [12] G. Hinton, P. Dayan, and M. Revow, "Modelling the manifolds of images of handwritten digits," *IEEE Trans. Neural Networks*, vol. 8, no. 1, pp. 65–74, 1997.
- [13] C. Bachmann, T. Ainsworth, and R. Fusina, "Exploiting manifold geometry in hyperspectral imagery," *IEEE Trans. Geosci. Remote Sens.*, vol. 43, no. 3, pp. 441–454, 2005.
- [14] R. Schmidt, "Multilinear array manifold interpolation," *IEEE Trans. Signal Process.*, vol. 40, no. 4, pp. 857–866, 1992.
- [15] F. Belloni, A. Richter, and V. Koivunen, "DOA estimation via manifold separation for arbitrary array structures," *IEEE Trans. Signal Process.*, vol. 55, no. 10, pp. 4800–4810, 2007.
- [16] Y. Wu, K. Wong, and S.-K. Lau, "The acoustic vector-sensor's near-field array-manifold," *IEEE Trans. Signal Process.*, vol. 58, no. 7, pp. 3946–3951, 2010.
- [17] D. Shuman, S. Narang, P. Frossard, A. Ortega, and P. Vandergheynst, "The emerging field of signal processing on graphs: Extending high-dimensional data analysis to networks and other irregular domains," *IEEE Signal Process. Mag.*, vol. 30, no. 3, pp. 83–98, 2013.
- [18] A. Sandryhaila and J. Moura, "Discrete signal processing on graphs," *IEEE Trans. Signal Process.*, vol. 61, no. 7, pp. 1644–1656, 2013.
- [19] J. Costa and A. Hero, "Geodesic entropic graphs for dimension and entropy estimation in manifold learning," *IEEE Trans. Signal Process.*, vol. 52, no. 8, pp. 2210–2221, 2004.
- [20] S. Roweis and L. Saul, "Nonlinear dimensionality reduction by locally linear embedding," *Science*, vol. 290, no. 5500, pp. 2323–2326, 2000.
- [21] Z. Zhang and H. Zha, "Principal manifolds and nonlinear dimensionality reduction via tangent space alignment," *SIAM J. Sci. Comp.*, vol. 26, no. 1, pp. 313–338, 2004.
- [22] J. Tenenbaum, V. De Silva, and J. Langford, "A global geometric framework for nonlinear dimensionality reduction," *Science*, vol. 290, no. 5500, pp. 2319–2323, 2000.
- [23] M. Belkin and P. Niyogi, "Laplacian eigenmaps for dimensionality reduction and data representation," *Neural Comp.*, vol. 15, no. 6, pp. 1373–1396, 2003.
- [24] P. Vepakomma and A. Elgammal, "A fast algorithm for manifold learning by posing it as a symmetric diagonally dominant linear system," *Appl. Comput. Harmon. Anal.*, vol. 40, no. 3, pp. 622–628, 2015.
- [25] R. Coifman and S. Lafon, "Diffusion maps," *Appl. Comput. Harmon. Anal.*, vol. 21, no. 1, pp. 5–30, 2006.
- [26] R. Talmon, I. Cohen, S. Gannot, and R. Coifman, "Diffusion maps for signal processing: A deeper look at manifold-learning techniques based on kernels and graphs," *IEEE Signal Process. Mag.*, vol. 30, no. 4, pp. 75–86, 2013.
- [27] Y. Yang, F. Nie, S. Xiang, Y. Zhuang, and W. Wang, "Local and global regressive mapping for manifold learning with out-of-sample extrapolation," in *Proc. AAAI Conf. Artificial Intell. (AAAI)*, 2010, pp. 649–654.
- [28] D. Cohn, Z. Ghahramani, and M. Jordan, "Active learning with statistical models," *J. Artificial Intell. Res.*, vol. 4, no. 1, pp. 129–145, 1996.
- [29] B. Settles, "Active learning literature survey," *Science*, vol. 10, no. 3, pp. 237–304, 1995.
- [30] D. Liang and J. Paisley, "Landmarking manifolds with Gaussian processes," in *Proc. Int. Conf. Mach. Learn. (ICML)*, 2015, pp. 466–474.
- [31] G. Schohn and D. Cohn, "Less is more: Active learning with support vector machines," in *Proc. Int. Conf. Mach. Learn. (ICML)*, 2000, pp. 839–846.
- [32] J. Paisley, X. Liao, and L. Carin, "Active learning and basis selection for kernel-based linear models: A Bayesian perspective," *IEEE Trans. Signal Process.*, vol. 58, no. 5, pp. 2686–2700, 2010.
- [33] T. Tsiligkaridis, B. Sadler, and A. Hero, "On decentralized estimation with active queries," *IEEE Trans. Signal Process.*, vol. 63, no. 10, pp. 2610–2622, 2015.
- [34] S. Vijayanarasimhan and K. Grauman, "Large-scale live active learning: Training object detectors with crawled data and crowds," *Int. J. Comput. Vis.*, vol. 108, no. 1–2, pp. 97–114, 2014.
- [35] C. Thompson, M. Califf, and R. Mooney, "Active learning for natural language parsing and information extraction," in *Proc. Int. Conf. Mach. Learn. (ICML)*, 1999, pp. 406–414.
- [36] G. Riccardi and D. Hakkani-Tur, "Active learning: Theory and applications to automatic speech recognition," *IEEE Trans. Speech Audio Process.*, vol. 13, no. 4, pp. 504–511, 2005.
- [37] L. Zhao, S. J. Pan, E. W. Xiang, E. Zhong, Z. Lu, and Q. Yang, "Active transfer learning for cross-system recommendation," in *Proc. AAAI Conf. Artificial Intell. (AAAI)*, 2013, pp. 1205–1211.
- [38] Y. Chen, M. Crawford, and J. Ghosh, "Improved nonlinear manifold learning for land cover classification via intelligent landmark selection," in *Proc. IEEE Int. Geosci. Remote Sens. Symp. (IGARSS)*, 2006, pp. 545–548.
- [39] J. Chi and M. Crawford, "Selection of landmark points on nonlinear manifolds for spectral unmixing using local homogeneity," *IEEE Geosci. Remote Sens. Lett.*, vol. 10, no. 4, pp. 711–715, 2013.
- [40] —, "Active landmark sampling for manifold learning based spectral unmixing," *IEEE Geosci. Remote Sens. Lett.*, vol. 11, no. 11, pp. 1881–1885, 2014.
- [41] V. De Silva and J. Tenenbaum, "Sparse multidimensional scaling using landmark points," Stanford University, Tech. Rep., 2004.
- [42] J. Silva, J. Marques, and J. Lemos, "Selecting landmark points for sparse manifold learning," in *Proc. Conf. Neural Inform. Process. Systems (NIPS)*, 2006, pp. 1241–1248.
- [43] C. Wachinger and P. Golland, "Diverse landmark sampling from determinantal point processes for scalable manifold learning," *arXiv:1503.03506*, 2015.
- [44] G. Golub and C. Van Loan, *Matrix computations*. Baltimore, MD: JHU Press, 1996.
- [45] R. Braatz and M. Morari, "Minimizing the Euclidean condition number," *SIAM J. Control Optim.*, vol. 32, no. 6, pp. 1763–1768, 1994.
- [46] C. Greif and J. Varah, "Minimizing the condition number for small rank modifications," *SIAM J. Matrix Anal. Appl.*, vol. 29, no. 1, pp. 82–97, 2006.
- [47] Z. Lu and T. Pong, "Minimizing condition number via convex programming," *SIAM J. Matrix Anal. Appl.*, vol. 32, no. 4, pp. 1193–1211, 2011.
- [48] X. Chen, R. Womersley, and J. Ye, "Minimizing the condition number of a Gram matrix," *SIAM J. Optim.*, vol. 21, no. 1, pp. 127–148, 2011.

- [49] Y.-P. Hong and C.-T. Pan, "Rank-revealing QR factorizations and the singular value decomposition," *Math. Comp.*, vol. 58, no. 197, pp. 213–232, 1992.
- [50] J. Ahlberg and E. Nilson, "Convergence properties on the spline fit," *J. SIAM*, vol. 11, no. 1, pp. 95–104, 1963.
- [51] J. Varah, "A lower bound for the smallest singular value of a matrix," *Linear Algebra Appl.*, vol. 11, no. 1, pp. 3–5, 1975.
- [52] Z. Jiang, Z. Lin, and L. Davis, "Learning a discriminative dictionary for sparse coding via label consistent K-SVD," in *Proc. IEEE Conf. Comp. Vision and Pattern Recognition (CVPR)*, 2011, pp. 1697–1704.
- [53] A. Rahimi, T. Darrell, and B. Recht, "Learning appearance manifolds from video," in *Proc. IEEE Conf. Comp. Vision and Pattern Recognition (CVPR)*, 2005, pp. 868–875.
- [54] Y. Tian and S. Narasimhan, "Hierarchical data-driven descent for efficient optimal deformation estimation," in *Proc. IEEE Int. Conf. Comp. Vision (ICCV)*, 2013, pp. 2288–2295.
- [55] A. Martinez and R. Benavente, "The AR face database," Computer Vision Center, Tech. Rep. 24, 1998.
- [56] C. Cortes and V. Vapnik, "Support-vector networks," *Mach. Learn.*, vol. 20, no. 3, pp. 273–297, 1995.
- [57] P. Dollár, V. Rabaud, and S. Belongie, "Learning to traverse image manifolds," in *Proc. Conf. Neural Inform. Process. Systems (NIPS)*, 2006, pp. 361–368.
- [58] H. Xu and H. Zha, "Manifold based face synthesis from sparse samples," in *Proc. IEEE Int. Conf. Comp. Vision (ICCV)*, 2013, pp. 2208–2215.
- [59] H. Xu, H. Zha, and M. Davenport, "Manifold based dynamic texture synthesis from extremely few samples," in *Proc. IEEE Conf. Comp. Vision and Pattern Recognition (CVPR)*, 2014, pp. 3019–3026.